IEEE Access
Multidisciplinary | Rapid Review | Open Access Journal

Received October 20, 2019, accepted November 28, 2019, date of publication December 19, 2019,
date of current version January 17, 2020.

Digital Object Identifier 10.1109/ACCESS.2019.2961003

Prototype of a Morphological Positioning Robot for Radiology

RONGQIAN YANG[1,2,3], KAIYANG BAO[1], LINGXIANG ZHENG[1], YANGJIE XIE[1], AND PEIFENG GUAN[4]

[1]School of Materials Science and Engineering, South China University of Technology, Guangzhou 510006, China
[2]School of Medicine, Yale University, New Haven, CT 06520, USA
[3]Guangdong Engineering Technology Research Center for Translational Medicine of Mental Disorders, Guangzhou 510370, China
[4]Guangzhou Aimooe Technology Company, Ltd., Guangzhou 510006, China

Corresponding author: Rongqian Yang (bmeyrq@foxmail.com)

This work was supported in part by the National Natural Scientific Foundation of China under Grant 81671788, in part by the Guangdong Provincial Science and Technology Program under Grant 2017B020210008 and Grant 2017B010110015, in part by the Guangzhou Science and Technology Program under Grant 201704020228, and in part by the Chinese Scholarship Fund under Grant 201806155010.

ABSTRACT The accuracy of placement during radiotherapy significantly affects treatment quality. During the current and subsequent fractions of radiotherapy treatment (RTT), positional mismatching between the initial CT-scanned location and the current physical state reduces efficiency in RTT. In general, this situation requires doctors to perform freehand adjustment in RTT to adapt the current alteration of patients and guarantee the effectiveness of the plan, which is described as ''plan adapts to tumor,'' and is typically cumbersome. To mitigate such drawback, we designed a morphological robotic system that can keep a patient's posture identical with the first fraction. Furthermore, we directly adjusted nonrigid tumor deformation. Hence, the system achieved high-level matching accuracy between the current and initial physical states, which is notably described as ''tumor adapts to plan.'' Our proposed robotic system consists of a pilot circuit, morphological and mechanical structures, and operating software. A series of experiments was conducted to prove the feasibility and precision of the developed system. Results showed that the proposed robotic system can maintain the same posture as the first fraction. It exhibits the potential to become an efficient solution in radiotherapy.

INDEX TERMS Morphological robot, nonrigid deformation, placement, radiotherapy.

I. INTRODUCTION

Acomplete course of radiotherapy treatment (RTT) for a tumor is typically administered in different fractions over several weeks. During this period, RTT requires precise positioning, planning, verification, and implementation. Precise positioning, *i.e.*, precise matching between the clinical target volume (CTV) and the actual tumor area, is the premise of precise RTT and can be achieved in the first fraction. Ideally, the match of every RTT fraction between the placement of the patient and the initially planned CT should all be consistent with the first fraction to efficiently and effectively execute the radiotherapy plan based on the initially planned CT. Given the complexity of the human body system and human operator errors, tumor cannot reach the ideal state [1] of being identical with the first fraction. The major reasons for such failure include randomness when the patient is lying down and the involuntary movements of human organs during fractions [2], [3] (Fig. 1).

The associate editor coordinating the review of this manuscript and approving it for publication was Cristian A. Linte.

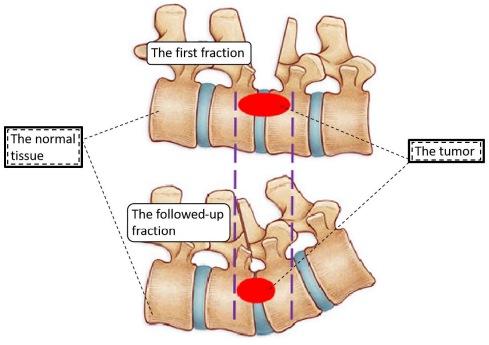

FIGURE 1. Illustration of tumor deformation via compression. After the first fraction, the tumor state may be influenced by compression or other factors, and thus, its shape or location may change and no longer match with the initially planned CT.

When a patient is treated in a fraction in the course of RTT, several significant parameters, such as tumor size, location, and shape, and the relationship between the tumor and the surrounding normal tissues and organs, will exhibit different degrees of changes. Moreover, no guarantee exists that all the aforementioned tumor parameters will be consistent with the initially planned CT. Under such adverse conditions, doctors and radiologists encounter difficulties in ensuring and improving the efficiency of RTT. Using the original plan will apparently lead to CTV dose change, decreasing the effect of RTT [4].

To solve the aforementioned problems, a sequence of image-guided radiotherapy (IGRT) systems [5] has been documented to select a series or parallel six degrees-of-freedom (DoF) robot as the movement unit of treatment couch (Fig. 2). For example, the Varian (six DoF placement treatment couch) is applicable to all requested shifts, including translational and rotational movements with high accuracy of up to 0.02 cm and 0.4°, on average, and no difference can be observed between tests with and without a couch load of up to 200 kg [6]. Although this type of device can achieve the calibration of overall rigidity error to a certain extent, it is insufficient for enabling RTT to reach a precise location to make a patient's posture identical with that in the first fraction. Moreover, nonrigid tumor deformation even shrivels the couch.

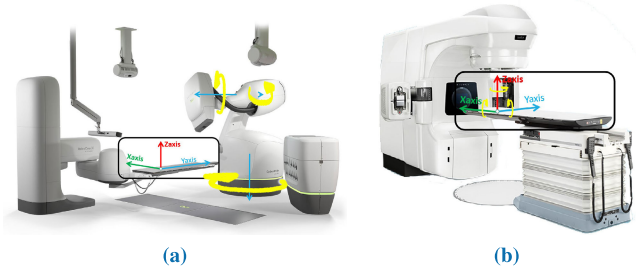

FIGURE 2. Common structure of a placement couch in a radiotherapy system. (a) Three DoF placement couch in a series structure. This couch completes three DoF linear displacement tasks in patient space. Simultaneously, the three DoF delivery robot that is working with the couch can fulfill the rotation task that consists of yaw, pitch, and roll transformation. Thus, it can accomplish complete placement in RTT. (b) Six DoF placement couch in a parallel structure. In contrast with the former, this couch can complete all six DoF movement tasks, including translation and rotation, to work with the delivery equipment to accomplish placement in RTT.

In such situation, an effective strategy is to place dunnage to adjust or fix local patient posture (Fig. 3). By using these materials, the doctor can indirectly correct nonrigid deformation. However, the use of dunnage exhibits limitations, such as material waste and location inaccuracy. Another useful method is initiative modifying the RTT plan; however, the revision of plan frequently requires the participation of physiologists and radiologists, which is burdensome and ineffective [7]–[10]. Accordingly, a more advanced technology, called online automatic adaptive radiotherapy (ART), was proposed [11], [12]. Among which, the most common is based on the cone beam comic computed tomography (CBCT) [13]–[16]. For example, the supercomputing online replanning environment (SCORE) GPU-based RTT planning and reoptimization system developed by the Southwest Texas Medical Center exhibits the function of automatic optimization for the RTT plan; this system performs accurate calculation of the radiological dose and the dose–volume histogram (DVH) curve of each voxel on a previous initially planned CT, CBCT, or optimized initially planned CT [17].

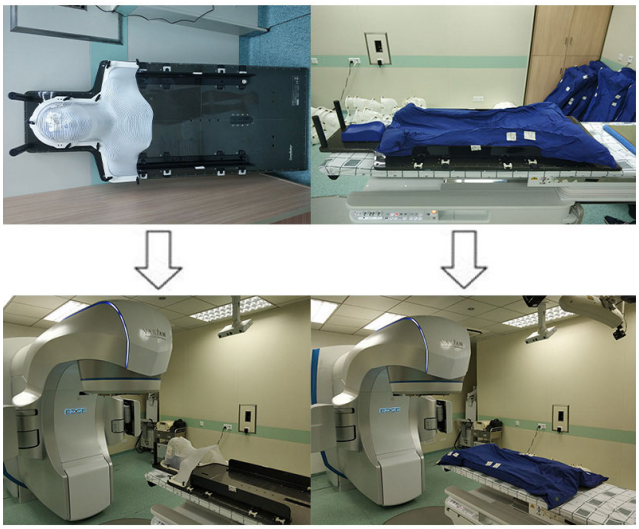

FIGURE 3. Correcting patient posture using dunnage or mesh enclosure on the couch. This figure explains the defect of the traditional couch. In an actual scenario, the doctor is frequently required to custom fit consumable items for each patient in accordance with different delivery parts of the body to fix patient posture during RTT. The head and neck neoplasm needs a scleroid mesh enclosure (top left corner of this figure). The doctor must always carry the board with the mesh enclosure to the couch (left bottom of this figure). In another case in which tumor is located in the trunk, doctors will similarly put dunnage (top right corner of this figure) on the couch to fix patient posture. Both materials are custom-designed for each patient to match his/her body shape, resulting in high overhead and are inconvenient to operate. These consumable items still require considerable manual intervention. Although RTT can be executed smoothly, the process is tedious and ineffective.

Several researchers have used SCORE to verify the statistics on its RTT performance with esophageal tumor. The results confirmed that the uniformity of dose distribution has been improved and the coverage of the target area has been increased by 7.56% compared with the original plan without optimization after qualifying the RTT plan. Furthermore, the dose in key organs was also significantly reduced. However, this method still requires a physician to manually delineate the target area for the current tumor during plan optimization and conduct experimental verification of the dose and location for a new radiotherapy plan before executing it, and thus, it is generally less automated. Consequently, patients do not receive RTT immediately after plan optimization, during which the dynamic motion of the patients may lead to new tumor deformation.

So the initiative optimization approach (i.e. plan adapts to the tumor) would not be adopted to low down the match error but we take into consideration the treatment couch.

Assuming that if the couch can generate an arbitrary surface, then at least two cruxes can be resolved. First, the dunnage can be replaced, and doctors do not have to design such material for each patient, saving considerable costs. Second, with the features of a flexible and arbitrary surface, doctors can adjust the posture of patients sufficiently, minimizing matching errors between the initially planned CT and the followed-up fractions. Such errors commonly occur in RTT. With regard to the generating surface, we found several devices to address the tactile and perception aspects [18], [19]. Most of these devices are used to contact information but we intend to use the generated surface to support and fix patients and perform optimized placement. Thus, we also combine medical image processing technology and consider the flexibility and variability of a morphological robot apart from the traditional technology used in electronic and mechanical engineering [20], to design an available system. Fig. 4 shows the conceptual machine design and 3D rendering model. The device has integrated a number of linear motor modules (LMM) to constitute the morphological robot that generates an arbitrary bearing surface to correct the posture of patients. The experimental results suggest that the bearing surface can loosen the mechanical constraints on any part of the body, keeping the patient's posture identical to that in the first fraction to the maximum extent and implementing adjustment on local posture.

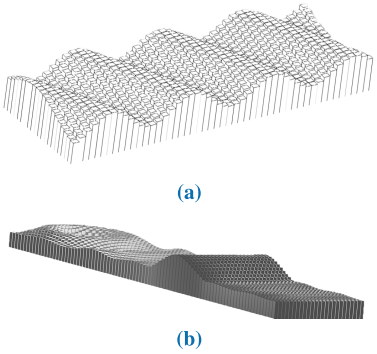

FIGURE 4. Morphological robotic component for generating an arbitrary support surface that can adapt to different body shapes, replace consumable items, improve the efficiency of RTT, and ease the burden of doctors. Hence, this morphological robotic component can replace the dunnage and bracket to fulfill the task of fixing patients during RTT. (a) Conceptual machine design and (b) 3D rendering model.

Furthermore, The morphological robot lays the foundation to achieve the purpose of ''tumor adapts to plan'' to avoid tedious optimization and verification caused by tumor deformation. Meanwhile, dynamic and accurate matching, i.e., not only tracking the tumor but also compensating for the deformation, can be realized simultaneously.

II. DEVICE DESIGN

We intend to assemble the morphological robot into the IGRT system to minimize tumor deformation. As shown in Fig. 5, the entire architecture with the bearing surface couch is our retrofitted morphological robot.

FIGURE 5. System architecture. The image shows how we utilize the robot in the available radiology system, i.e., the final version of the robot can be locked onto the carbon fiberboard. Instead of putting dunnage or mesh enclosure, the robot can generate different support surfaces for different body shapes. The doctors can also implement a more detailed adjustment for patient local posture by simply using electronic control. The robot can transform the placement process from manual intervention into semiautomated, saving material loss from fabricating dunnage and mesh enclosure.

We design a prototypical machine and use it to test the performance of RTT placement. The machine consists of the mechanical component for generating the bearing surface, electronic circuits for controlling the mechanical component, and software with user interface (UI) for doctors to analyze the bearing surface that should be generated.

A. HARDWARE

The device is fabricated from an aluminum frame, LMM, and control electronic circuits.

The LMM includes a stepper motor, a screw rod, two push rods, a linear guide rail, and a precision ball bearing linear slider. The screw rod is installed on the slider parallel to the linear guide rail. The stepper motor drives the screw rod to rotate, and then the slider and the push rod move back-and-forth together on the linear guide. The machine structure is shown in the left panel of Fig. 6a. Lastly, a support block is located at the top of the LMM, protruding out of the iron framework. All the aforementioned parts constitute a movement unit of the morphological robot. Meanwhile, the LMM can perform high-precision linear motion with an accuracy of up to 1–100th of a millimeter in one DoF.

All the LMMs contribute to forming an appropriate surface for precise RTT requirement. The ultimate appearance of the prototype is illustrated in the right panel of Fig. 6a. A number of LMMs are arranged vertically in a square array and fixed onto the aluminum frame through the assembly screw holes. During the initial state, the translated distance of each LMM is 0 mm, and thus, the entire robot presents a plane. Then, the robot can generate the right bearing surface under software control (Fig. 6b). The control's electronic circuit consists of serial port communication, data conversion, and morphological robot control.

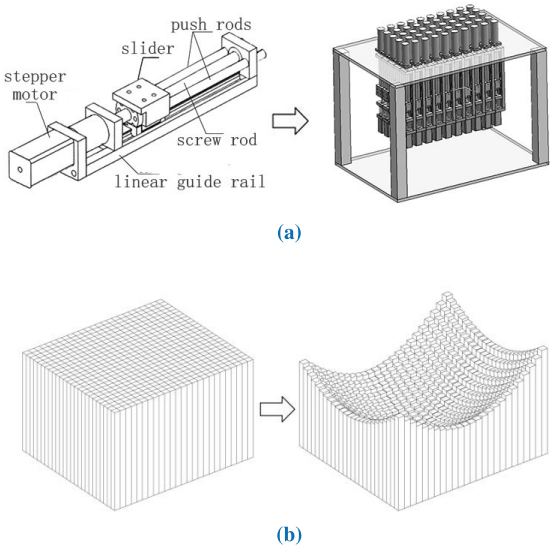

FIGURE 6. Constitution of the morphological component. (a) Structure of the LMM in the left panel and the total prototype in the right panel. The latter is assembled with a number of LMMs in an aluminum frame. (b) Action transformation.

B. SOFTWARE

In this part, we design a combined control system that comprises a host computer and a slave computer. The host computer includes the UI, the algorithm for bearing surface calculation, and a 3D image window for users to design a suitable bearing surface.

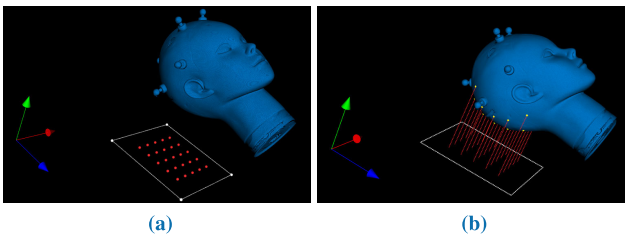

FIGURE 7. Application of 3D image window. (a) Rendering CT images and displaying stereo images. (b) When the algorithm completes its calculation, the data of the bearing surface are illustrated in red bars.

First, the main application of UI is to adjust the stereo image position and orientation in 3D. Second, the 3D image window is responsible for the reconstruction and visualization of a CT image sequence (Fig. 7a). Third, the algorithm calculates the movement distance of each LMM and illustrates the distance on the 3D image window (Fig. 7b). Moreover, serial port communication is used to send the distance data from the host computer to the slave computer, i.e., MCU.

III. METHOD

A. WORKFLOW DESIGN

We design a system workflow (Fig. 8) to make the posture of the patient correspond to that in the first fraction, and thus, reduce nonrigid deformation of the tumor. Fig. 8 presents our method and the system's architecture. The architecture has two major parts, namely, software and hardware.

First, a CT-scanned image sequence is imported into the workflow, providing the necessary information dataset and 2D image data. Subsequently, a 3D image is reconstructed using the Ray Casting method [21], [22]. Moreover, a fiducial plane where all the reference points are located is generated in image space. The size of this fiducial plane is in accord with that of the practical robot system in patient space. The process is summarized as Steps 1 to 4.

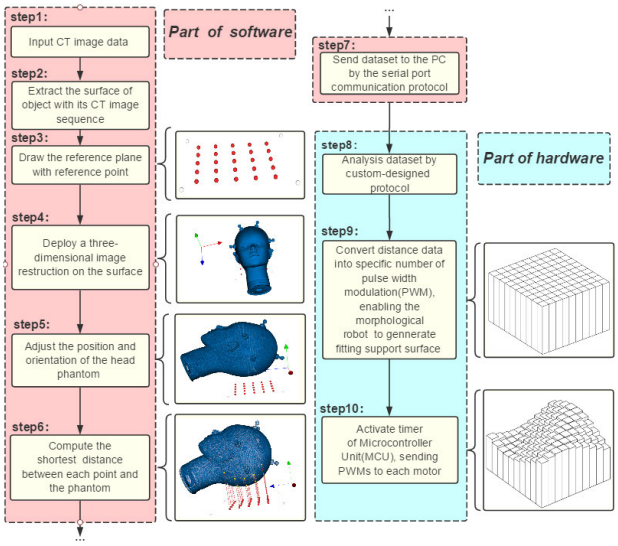

FIGURE 8. Workflow of the morphological robotic system. The first column sketch map in the left panel shows what happens in the display window when users operate the software. The right column shows what occurs with the robot component.

To determine the relative position and orientation between the reference plane and the CT-scanned object, the developed software provides users with position adjustment of the phantom in translation and orientation. The transformation result is shown in Step 5, where the backside of the CT-scanned object is located above the plane to enable the robot to generate the correct bearing surface to hold the object in practice.

Subsequently, the support distances with respect to the object are determined using the developed algorithm. Lastly, the serial port of the host computer opens and sends distance data to the slave computer, i.e., Step 6. Thus far, the software has accomplished the preparation work. The remaining task is controlling the composition of the morphological robot to generate the appropriate bearing surface. The slave computer works automatically without manual intervention. The sub-workflow is presented as follows. (1) The electronic circuit receives data from the host computer via serial port communication and saves them in the MCU's buffer as Step 8. (2) The MCU converts them to decimal numbers in Step 9 because data in the buffer is hexadecimal. The detail of the conversion is introduced in the next subsection. Then, the MCU uses the converted data to control its timer to produce pulse width modulation (PWM) signals. The number of pulses is specific for driving the robot such that an LMM can maintain more than two decimal precision. Lastly, given the PWM signals,

the robot drives all the LMMs to exhibit linear motion with the corresponding height.

B. ALGORITHMS

1) EXTRACTING THE SURFACE OF A 3D IMAGE

We develop a threshold-based algorithm to obtain the surface data of the CT-scanned object to create a perfect bearing surface (Alg. 1). The input of this algorithm is the image volume data and the threshold range of the surface; the output is the target surface. The segmentation principle is based on the judgment of a six neighborhood point set (SNP), confirming that the SNP of a point belongs to the surface with less than six points and whose HU value satisfies the threshold range (Fig. 9).

Algorithm 1 Extract the Surface of CT Image Data

Input: The original three-dimensional CT image data Q_n, which is a point set; HU value range of surface $Thred_d < C_m < Thred_u$.

Output: Surface image data Qs_n. .

1: Importing Q_n;

2: Extracting the surface of object:

3: **for** m = 0, m< number of Q_n, m++ **do**

pick a point $Q_m(x_m, y_m, z_m)$ from Q_n;

4: **if** more than one points of

$$\begin{cases} Q_{mx}(x_m+1, y_m, z_m) \\ Q_{my}(x_m, y_m+1, z_m) \\ Q_{mz}(x_m, y_m, z_m+1) \\ Q_{-mx}(x_m-1, y_m, z_m) \\ Q_{-my}(x_m, y_m-1z_m) \\ Q_{-mz}(x_m, y_m, z_m-1) \end{cases}$$

whose HU value are unsatisfied with $Thred_d < C_m < Thred_u$ **then** saving Q_m in Qs_n

5: **end if**

6: **end for**

return Qs_n;

2) COMPUTING THE MOVEMENT DISTANCE OF EACH LMM

The optimized bearing surface can be found by Alg. 2, which calculates the vertical distance from every reference point to the surface. However, the coordinate of a reference point lies on the $X - Y$ plane, and the surface data are preserved in the form of a point set, and thus, the surface data have no analytic expression. Accordingly, we cannot find the vertical distance by using the analytic geometry method or by directly solving equations (Fig. 10a). An indirect method is to find the point on the surface that satisfies the aforementioned conditions. Thus, our method can be realized by using an iterative strategy (Fig. 10b).

In the iterative method, we compare the X and Y coordinates of the two point sets that belong to the surface

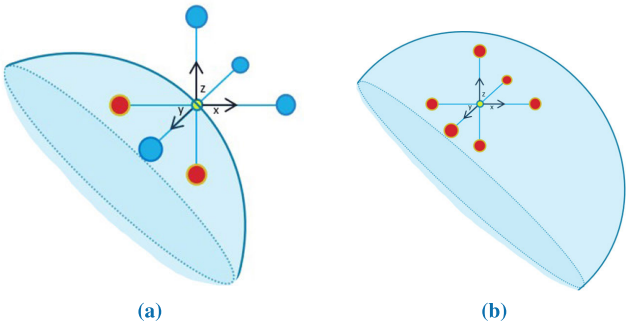

FIGURE 9. Determining whether a point is on the surface of a CT-scanned object. (a) Scenario in which a point is located on the surface of a CT-scanned object. Four points are located on the external surface and two points are located on the internal surface for the neighborhood of yellow points. Under our conditions, this point is located on the surface. (b) Scenario in which a point is located on the internal surface. All the neighborhoods are located on the internal surface. Therefore, the yellow points are located on the internal surface. In particular, we adjust the proportion between each neighbor point and surface appropriately. Moreover, all the intervals between the neighbor point and the center point is the minimum value (i.e., 1 pixel). Hence, our judgment criterion is necessary and sufficient.

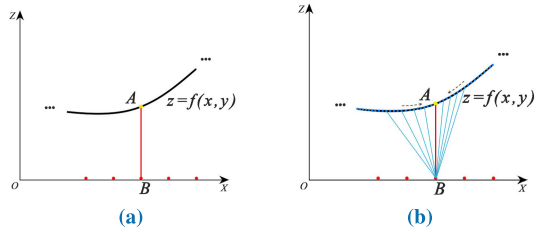

FIGURE 10. Two different methods to find point *A*. The two diagrams take from $X - Z$ plane at $Y = y_0$, curve z belongs to the CT-scanned object, ellipsis represents the other part of CT-scanned object which is no need to exhibit here. (a) The method of analytic geometry to find point *A* on curve *z*, which need to know analytic expression of the curve *z*. (b) The iterative method in which we compare all points of the surface with single reference point *B* until find point *A*, and the segment *AB* is perpendicular to reference plane.

point set and the reference plane. If both arguments are extremely close, i.e., their difference is sufficiently small such that segment AB is perpendicular to the $X - Y$ plane, then many points satisfy the aforementioned constraint conditions. Furthermore, we select from these possible points by determining the minimum calculated distance. Consequently, we deal with the other points of reference on the plane by using a multi-thread strategy. Lastly, we obtain the complete dataset of the robotic bearing surface.

3) DATA CONVERSION

We need to convert the decimal data from real distances to the specific number of PWM to control each LMM and generate identical surfaces. The MCU can control the LMMs to perform appropriate rectilinear translation by working with the other parameters, such as stepper angle and subdivision of the stepper motor (Alg. 3). Notably, we open several timers and their channels. $Count_n$ represents all the channels of a timer, and $Count_x$ represents one $Count_n$.

Algorithm 2 Compute Movement Distance of Every Stepper Motor Module

Input: The surface CT image data Qs_n.

Output: Distance dataset h_n;

Importing Qs_n;

Parameterizing the reference plane with reference point set $P_{(m,n)}$;

Three-dimensional reconstructing Qs_n and $Surface_p$ rendering in window;

repeat

Freehand operation:

$$\begin{cases} Surface_p = R_k * Surface_p + T_k \\ Qs_n = R_k * Surface_p + T_k \end{cases}$$

where $k \in \{x, y, z\}$;

until The posture corresponds to the initial CT-scanned posture;

Deploy on the following step of 7-14 by using multi-thread strategy, the number of thread is mn;

for h $= 0$, h$<$ number of Qs_n, h$++$ **do**

$V_x = Qs_h^x - P_{(i,j)}^x$;

$V_y = Qs_h^y - P_{(i,j)}^y$;

where Qs_a^b represent the component of "a" axis of the "bth" point of Qs_n, similarly, $P_{(i,j)}^e$ represent the component of "e" axis of point $P_{(i,j)}$.

if $|V_x| < 1$ && $|V_y| < 1$ **then**

Calculating the distance L_t^2, $t = 0$, $t \in N^*$ from $P_{(i,j)}$ to Q_h: $L_t^2 = \left(Q_h^x - P_{(i,j)}^x\right)^2 + \left(Q_h^y - P_{(i,j)}^y\right)^2 + \left(Q_h^z - P_{(i,j)}^z\right)^2$;

if $L_t^2 < L_{t-1}^2$ **then**

$L_{t-1}^2 = L_t^2$;

$t++$;

if $h =$number of Q_n **then**

Saving $\sqrt{L_{t-1}^2}$ in list h_n;

end if

end if

end if

end for

return h_n;

Algorithm 3 Convert the Data of Distance From USART Buffer for Robot to Generate Right Surface

Input: First address of buffer AD_h which has been preserved distance data h_n that is metric and keep two decimals;

Output: The number of PWM H_n which can be used to generate specific driving signal; The accurate control signal;

Opening the serial port of slave computer, receiving data h_n from host computer, saving data in USART buffer;

Converting data from buffer:

for i $= 0$, i $< mn$, i$++$ **do**

$$H_i = \frac{Sub_m}{100}(100\mathrm{AD_h}[2\mathrm{i}] + \mathrm{AD_h}[2\mathrm{i}+1]);$$

where $\frac{Sub_m}{100}$ is the subdivision of stepper motor.

end for

Starting timers, counting number of pulse denoted with $Count_n$;

repeat

for every channel of timers: $Count_x++$;

until $Count_x == H_x$;

Turning of timer for whose counting task has been finished.

IV. EXPERIMENT

A. PHANTOM PLACEMENT TESTING

We designed the experimental phantom and conducted a CT-scan to evaluate the feasibility of the robot, and then processed the image data with VTK [23] to make them visible (Fig. 11a). We performed a series of experiments on our system (Fig. 11b).

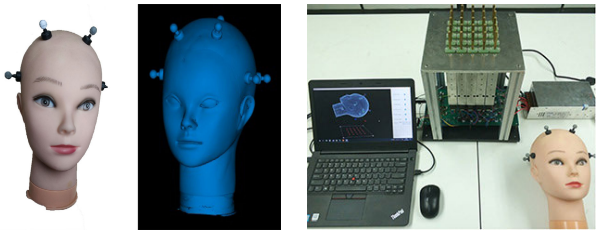

(a) (b)

FIGURE 11. The experimental platform. (a) The phantom used in experiment and its 3D image. (b) The picture of practical system architecture.

Using our proposed method, the morphological component generated the bearing surface that is supposed to match exactly with the phantom. The experimental result showed that goodness of fit with the surface of phantom was achieved (Fig. 12). The bar at the periphery came in contact with the surface of phantom. In particular, each support bar was close to the surface.

The morphological component matched with the phantom surface, with a significance that enables us to adjust the posture of patients in the initial state, i.e., the placement posture of the first fraction for RTT. Moreover, the morphological component eliminated the matching error between the planned CT and the actual state of the tumor because of the uncertainty that occurs when patients are lying down. Doctors can also apply detailed adjustments to the state of the internal tumor by using arbitrary DoF to obtain an accurate location in accordance with CBCT.

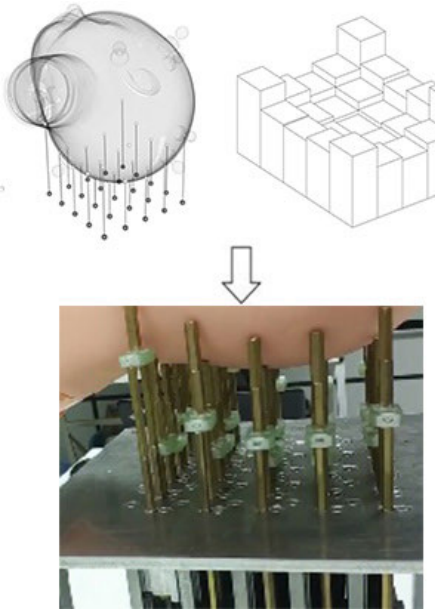

FIGURE 12. Desired bearing surface and experimental result in the practical scenario.

B. ACCURACY MEASUREMENT

We used an infrared camera to collect the 3D coordinates of each vertex of a bar to measure the accuracy of the placement result. In particular, we placed retro-reflective markers on its top vertex (Fig. 13a), and then used the infrared camera Eyeposition manufactured by Aimooe to collect the 3D coordinates of each point (Fig. 13b).

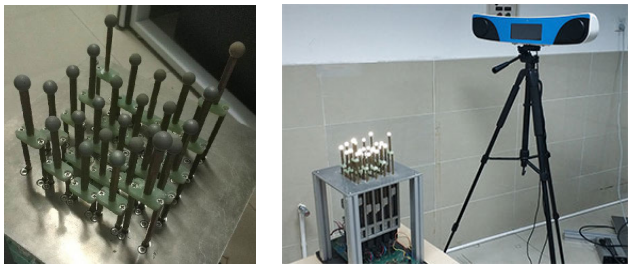

FIGURE 13. Collection of coordinate data. (a) Retro-reflective markers assembled on the robot. (b) Coordinates of every vertex collected by the infrared camera.

Then, we obtained the data of coordinates from Eyeposition and transformed the point set to correspond with the imaging space (Fig. 14). We transformed the point set using Rodrigues' rotation formula to make the coordinates of the points decouple with the current coordinate system (step2 in Fig. 14). Then, we transformed the points to make them suitable for our medical image space wherein the green points are the final completed point sets. Subsequently, we calculated the statistical error of the practical bearing's surface match with the phantom's surface (step4 in Fig. 14).

The distance error was analyzed (Fig. 15). As shown in Fig. 15, the mean error was within 0.5 mm, the standard deviation (SD) was within 0.1 mm, and the root-mean-square

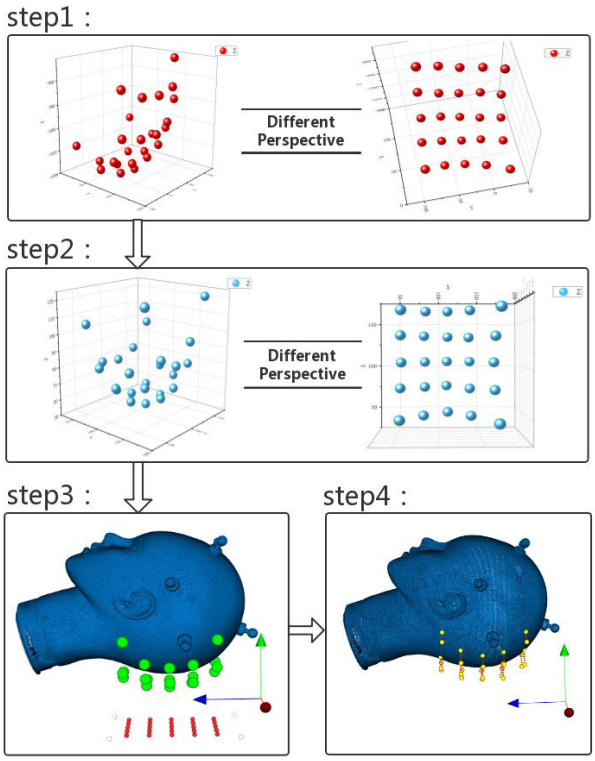

FIGURE 14. Process of dealing with the coordinate data.

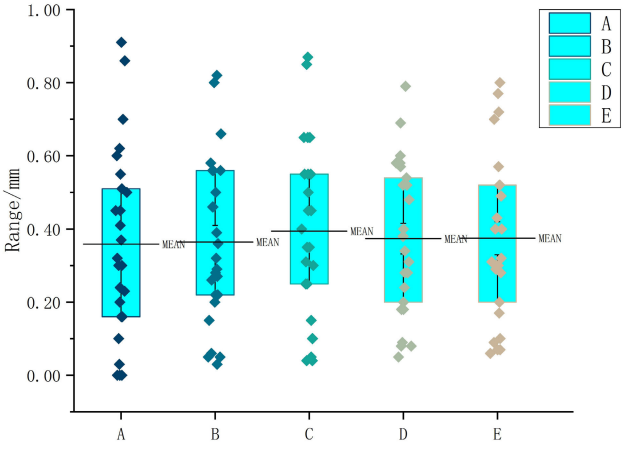

FIGURE 15. The statistical error of distance from bearing surface to phantom surface.

error (RMSE) was 0.44 ± 0.02 mm. The results satisfy the clinical requirements of RTT.

C. PHYSICAL PLACEMENT TESTING

Lastly, we tested positional accuracy in the human body. The experimental procedure is similar to the phantom placement test. We performed a CT-scan on a test subject and verified the practical results (Fig. 16). The results showed that the bearing surface exactly matched the human body. The posture of the test head was retained in the same position as that during the initial state before the CT-scan. The touch error can be further reduced due to the softness of skin, suggesting that the effects

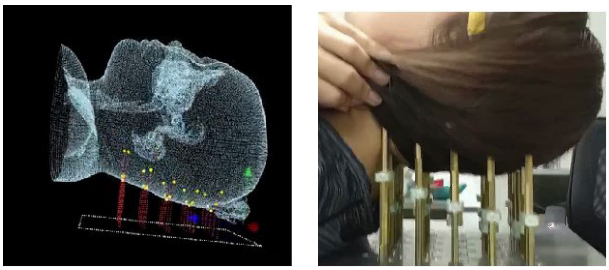

(a) (b)

FIGURE 16. Physical experiment. (a) Result of dealing with a test subject in image space. (b) Matching verification in practical scenario.

on the human body are better than those on the phantom in terms of error statistics. Despite the discouraging comfort level in the human subject test, the proposed system achieved novel performance in RTT placement. In our future work, the comfort of the couch will be improved using advanced materials.

V. CONCLUSION AND FUTURE WORK

In this work, we are inspired by haptics technologies and propose a new method for dealing with the placement task in radiology. The majority of the results indicate the remarkable feasibility and advantages of the system. The design and evaluation of the robotic morphological system for RTT are presented. As mentioned earlier, this robot cannot only save costs in dunnage fabrication but can also avoid matching errors between the initially planned CT and the follow-up fractions, which is the most common and challenging problem during RTT. In contrast with the types of equipment used in haptics, we particularly consider medical image processing with CT/MRI and matching precision, ensuring that the robot can be a potentially powerful tool in radiology placement. Our method is highly convenient to perform and can deal with difficult situations in radiology. The experimental results show that the robot maintains and adjusts the patient's posture locally, limiting tumor state to correspond with the first fraction. Thus, the efficiency of RTT is increased because the actual tumor state is highly matched with the initially planned CT during each fraction. In addition, the system can also eliminate repeated quality assurance on account of replanning the RTT. When the device undergoes a series of normalized improvements to meet the requirements of medical instrument standards until the system passes China Food and Drug Administration's certification and can be used in RTT, we will design and conduct experiments in real clinical situations to systematically compare this new method with available positioning techniques. Then, we can present the validity of our method in more detailed aspects, such as accuracy and terminal therapeutic effect based on actual experimental data. Future studies will consider respiratory tracking because the real-time placement of tumor during fraction is also a key factor that affects RTT efficiency. Lastly, we will incorporate the computer vision technique and complex control algorithms to improve the accuracy of the robot and enable it to perform more complicated functions, such as dynamic tracking in delivery treatment.

REFERENCES

[1] M. Vanherk, "Errors and margins in radiotherapy," *Seminars Radiat. Oncol.*, vol. 14, no. 1, pp. 52–64, Jan. 2004.
[2] P. J. Keall, G. S. Mageras, J. M. Balter, R. S. Emery, K. M. Forster, S. B. Jiang, J. M. Kapatoes, D. A. Low, M. J. Murphy, B. R. Murray, and C. R. Ramsey, "The management of respiratory motion in radiation oncology report of AAPM task group 76 a," *Med. Phys.*, vol. 33, no. 10, pp. 3874–3875, 2006.
[3] H. Fakir, L. Hlatky, H. Li, and R. Sachs, "Repopulation of interacting tumor cells during fractionated radiotherapy: Stochastic modeling of the tumor control probability," *Med. Phys.*, vol. 40, no. 12, Nov. 2013, Art. no. 121716.
[4] A. Vestergaard, L. P. Muren, H. Lindberg, K. L. Jakobsen, J. B. B. Petersen, U. V. Elstrøm, M. Agerbæk, and M. Høyer, "Normal tissue sparing in a phase II trial on daily adaptive plan selection in radiotherapy for urinary bladder cancer," *Acta Oncologica*, vol. 53, no. 8, pp. 997–1004, Aug. 2014.
[5] W. Cheon, J. Cho, S. H. Ahn, Y. Han, and D. H. Choi, "High-precision quality assurance of robotic couches with six degrees of freedom," *Phys. Medica*, vol. 49, pp. 28–33, May 2018.
[6] D. Schmidhalter, M. K. Fix, M. Wyss, N. Schaer, P. Munro, S. Scheib, P. Kunz, and P. Manser, "Evaluation of a new six degrees of freedom couch for radiation therapy," *Med. Phys.*, vol. 40, no. 11, Oct. 2013, Art. no. 111710.
[7] R. Marants, E. Vandervoort, and J. Cygler, "Dose and position quality assurance using the radpos system for 4D radiotherapy with cyberknife," in *Proc. World Congr. Med. Phys. Biomed. Eng.* Toronto, ON, Canada: Springer, Jun. 2015, pp. 599–602.
[8] S. W. Hadley, M. L. Kessler, D. W. Litzenberg, C. Lee, J. Irrer, X. Chen, E. Acosta, G. Weyburne, W. Keranen, K. Lam, E. Covington, K. C. Younge, M. M. Matuszak, and J. M. Moran, "SafetyNet: Streamlining and automating QA in radiotherapy," *J. Appl. Clin. Med. Phys.*, vol. 17, no. 1, pp. 387–395, Jan. 2016.
[9] L. Van Battum, D. Hoffmans, S. Kwa, and S. Heukelom, "Accuracy of Gafchromic EBT film as dose meter in radiotherapy QA," in *Proc. World Congr. Med. Phys. Biomed. Eng.* Munich, Germany: Springer, Sep. 2009, pp. 105–108.
[10] S. C. Vieira, R. S. J. P. Kaatee, M. L. P. Dirkx, and B. J. M. Heijmen, "Two-dimensional measurement of photon beam attenuation by the treatment couch and immobilization devices using an electronic portal imaging device," *Med. Phys.*, vol. 30, no. 11, pp. 2981–2987, Oct. 2003.
[11] S. Acharya, B. W. Fischer-Valuck, R. Kashani, P. Parikh, D. Yang, T. Zhao, O. Green, O. Wooten, H. H. Li, Y. Hu, V. Rodriguez, L. Olsen, C. Robinson, J. Michalski, S. Mutic, and J. Olsen, "Online magnetic resonance image guided adaptive radiation therapy: First clinical applications," *Int. J. Radiat. Oncol. Biol. Phys.*, vol. 94, no. 2, pp. 394–403, Feb. 2016.
[12] X. Han and Y. Zhou, "Three dimensional localization and tracking for adaptive radiation therapy," U.S. Patent 10 188 874 B2, Jan. 29, 2019.
[13] L. E. Court, L. Dong, A. K. Lee, R. Cheung, M. D. Bonnen, J. O'Daniel, H. Wang, R. Mohan, and D. Kuban, "An automatic CT-guided adaptive radiation therapy technique by online modification of multileaf collimator leaf positions for prostate cancer," *Int. J. Radiat. Oncol. Biol. Phys.*, vol. 62, no. 1, pp. 154–163, May 2005.
[14] M. Peroni, D. Ciardo, M. F. Spadea, M. Riboldi, S. Comi, D. Alterio, G. Baroni, and R. Orecchia, "Automatic segmentation and online virtualCT in head-and-neck adaptive radiation therapy," *Int. J. Radiat. Oncol. Biol. Phys.*, vol. 84, no. 3, pp. e427–e433, Nov. 2012.
[15] C. Kontaxis, G. H. Bol, J. J. W. Lagendijk, and B. W. Raaymakers, "A new methodology for inter-and intrafraction plan adaptation for the MR-linac," *Phys. Med. Biol.*, vol. 60, no. 19, pp. 7485–7497, Oct. 2015.
[16] J. J. W. Lagendijk, B. W. Raaymakers, and M. van Vulpen, "The magnetic resonance imaging-linac system," *Seminars Radiat. Oncol.*, vol. 24, no. 3, pp. 207–209, Jul. 2014.
[17] Q. Gautier, Z. Tian, Y. Graves, N. Li, M. Zarepisheh, C. Sutterley, F. Shi, L. Cervino, X. Jia, and S. Jiang, "TH-C-137-10: Development of a GPU research platform for automatic treatment planning and adaptive radiotherapy re-planning," *Med. Phys.*, vol. 40, p. 534, Jun. 2013.
[18] H. Iwata, H. Yano, F. Nakaizumi, and R. Kawamura, "Project FEELEX: Adding haptic surface to graphics," in *Proc. 28th Annu. Conf. Comput. Graph. Interact. Techn.*, 2001, pp. 469–476.

[19] K. Nakagaki, L. Vink, J. Counts, D. Windham, D. Leithinger, S. Follmer, and H. Ishii, "Materiable: Rendering dynamic material properties in response to direct physical touch with shape changing interfaces," in *Proc. CHI Conf. Hum. Factors Comput. Syst.*, 2016, pp. 2764–2772.
[20] K. Urai, R. Sawada, N. Hiasa, M. Yokota, and F. Dallalibera, "Design and control of a ray-mimicking soft robot based on morphological features for adaptive deformation," *Artif. Life Robot.*, vol. 20, no. 3, pp. 237–243, Oct. 2015.
[21] C. Silva and J. Mitchell, "The lazy sweep ray casting algorithm for rendering irregular grids," *IEEE Trans. Vis. Comput. Graphics*, vol. 3, no. 2, pp. 142–157, Apr./Jun. 1997.
[22] S. D. Roth, "Ray casting for modeling solids," *Comput. Graph. Image Process.*, vol. 18, no. 2, pp. 109–144, Feb. 1982.
[23] W. Schroeder, L. Avila, and W. Hoffman, "Visualizing with VTK: A tutorial," *IEEE Comput. Graph. Appl.*, vol. 20, no. 5, pp. 20–27, Sep./Oct. 2000.

RONGQIAN YANG received the B.S. degree in electronic instrumentation and measurement from Nanchang Hangkong University, Nanchang, China, in 2001, the M.S. degree in communication and information systems from Jinan University, Guangzhou, China, in 2005, and the Ph.D. degree in biomedical engineering from Shanghai Jiao Tong University, Shanghai, China, in 2009. He is currently an Associate Professor with the School of Materials Science and Engineering, South China University of Technology, Guangzhou. He is also the Vice Director of the Guangdong Engineering Technology Research Center for Translational Medicine of Mental Disorders, Guangzhou, and a Visiting Associate Professor with the Department of Therapeutic Radiology, Yale University, New Haven, CT, USA. His main research interests include medical robotics and biomedical instruments.

KAIYANG BAO received the B.S. degree in biomedical engineering from Changzhi Medical College, Changzhi, China, in 2017. He is currently pursuing the M.S. degree with the School of Materials Science and Engineering, South China University of Technology, Guangzhou, China. His main research interests include computer vision, medical image visualization, and robotics.

LINGXIANG ZHENG received the B.S. degree in biomedical engineering from the South China University of Technology, Guangzhou, China, in 2018, where he is currently pursuing the M.S. degree with the School of Materials Science and Engineering. His main research interests include computer vision, medical image visualization, and robotics.

YANGJIE XIE received the B.S. degree in biomedical engineering from the South China University of Technology, Guangzhou, China, in 2017, where she is currently pursuing the M.S. degree with the School of Materials Science and Engineering. Her main research interests include computer vision, medical image visualization, and robotics.

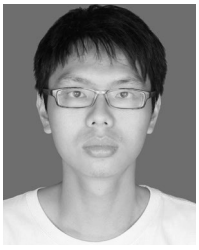

PEIFENG GUAN received the B.S. and M.S. degrees in biomedical engineering from the South China University of Technology, Guangzhou, China, in 2013 and 2016, respectively. He is currently an Engineer with Guangzhou Aimooe Technology Company, Ltd. His main research interests include surgical navigation systems and robotics.